

Extended Finite Elements for 3D-1D coupled problems via a PDE-constrained optimization approach

Denise Grappein ^{*}, Stefano Scialó [†], Fabio Vicini [‡]

Dipartimento di Scienze Matematiche, Politecnico di Torino, Corso Duca degli Abruzzi 24,
10129 Torino, Italy. Member of INdAM research group GNCS.

March 15, 2022

Abstract

In this work we propose the application of the eXtended Finite Element Method (XFEM) to the simulation of coupled elliptic problems on 3D and 1D domains, arising from the application of geometrical reduction models to fully three dimensional problems with cylindrical, or nearly cylindrical, inclusions with small radius. In this context, the use of non conforming meshes is widely adopted, even if, due to the presence of singular source terms for the 3D problems, mesh adaptation near the embedded 1D domains may be necessary to improve solution accuracy and to recover optimal convergence rates. The XFEM are used here as an alternative to mesh adaptation. The choice of a suitable enrichment function is presented and an effective quadrature strategy is proposed. Numerical tests show the effectiveness of the approach.

Keywords

3D-1D coupled problems, non conforming meshes, extended finite elements, numerical quadrature

1 Introduction

Coupled partial differential equation problems on 3D and 1D domains arise from the application of dimensional reduction models to equi-dimensional problems where cylindrical or nearly-cylindrical inclusions with small cross sectional size are embedded in a larger 3D domain, [11, 13, 1]. Indeed, the treatment of such narrow and elongated regions as one-dimensional manifolds reduces the overhead in simulations related to the generation of a computational mesh inside the inclusions. On the other hand, the mathematical formulation of 3D-1D coupled problems requires non standard approaches, and specialized numerical schemes are needed to correctly account for the presence of singularities [8, 9, 7, 12, 3]. The use of a 3D mesh non conforming to

^{*}denise.grappein@polito.it

[†]stefano.scialo@polito.it

[‡]fabio.vicini@polito.it

the 1D domains is quite a standard in the available approaches, but, in some cases, sub-optimal convergence rates are observed unless adaptive refinement close to the singularity is used, see e.g. [9, 10].

In this work we propose the use of the eXtended Finite Element Method (XFEM) for 3D-1D coupled problems as a means to avoid mesh refinement in the neighbourhood of the inclusions, thus improving the approximation capabilities and the accuracy of the solution avoiding the introduction of a large number of mesh cells, which could be unfeasible in realistic problems with a large number of inclusions. The use of XFEM for 3D problems with singular sources has been proposed also in [8], for quasi 3D problems for the simulation of the effect of well leakage in aquifers. Here, the methodology is extended to fully 3D-1D coupled problems, with an enrichment function chosen accordingly to the results provided in [7], and proposing an original quadrature scheme in this context. The PDE constrained formulation proposed in [1] is chosen for the 3D-1D problem.

We recall here the problem of interest and its formulation as a PDE constrained optimization formulation, referring to [1] for the details. A convex domain $\Omega \subset \mathbb{R}^3$ is considered with an embedded thin cylindrical region $\Sigma \subset \Omega$ of radius R smaller than the typical size of the domain and smaller than cylinder length. The boundary of Ω is $\partial\Omega$, whereas the boundary of Σ is denoted by Γ . The centreline of the cylinder is $\Lambda = \{\lambda(s), s \in [0, S]\}$, and $\Sigma(s), s \in [0, S]$ is a generic section, being instead Σ_0 and Σ_S the two end sections of Σ . For simplicity we assume that $\{\Sigma_0 \cup \Sigma_S\} \subset \partial\Omega$, and being $D = \Omega \setminus \Sigma$, we denote by $\partial D^e = \partial\Omega \setminus \{\Sigma_0 \cup \Sigma_S\}$ the external boundary of this region. A diffusion problem is considered in such domain, with unknown pressures $u \in D$ and $\tilde{u} \in \Sigma$:

$$-\nabla \cdot (K\nabla u) = f \quad \text{in } D \quad (1) \quad -\nabla \cdot (\tilde{K}\nabla \tilde{u}) = g \quad \text{in } \Sigma \quad (5)$$

$$u = 0 \quad \text{on } \partial D^e \quad (2) \quad \tilde{u} = 0 \quad \text{on } \Sigma_0 \cup \Sigma_S \quad (6)$$

$$u|_{\Gamma} = \psi \quad \text{on } \Gamma \quad (3) \quad \tilde{u}|_{\Gamma} = \psi \quad \text{on } \Gamma \quad (7)$$

$$K\nabla u \cdot \mathbf{n} = \phi \quad \text{on } \Gamma \quad (4) \quad \tilde{K}\nabla \tilde{u} \cdot \tilde{\mathbf{n}} = -\phi \quad \text{on } \Gamma \quad (8)$$

where homogeneous Dirichlet boundary conditions are prescribed on both $\partial\Omega, \Sigma_0$ and Σ_S . Being \mathbf{n} and $\tilde{\mathbf{n}} = -\mathbf{n}$ the outward pointing unit normal vectors to Γ , respectively for D and Σ , variable ϕ denotes the unknown flux through the interface Γ entering in D , while ψ is the unknown value of the pressure on Γ . Parameters K and \tilde{K} are positive scalars, while f and g are given source terms. Following [1] the above 3D-3D coupled problem is recast in a 3D-1D coupled problem, by means of a suitable choice of function spaces for the solution. Indeed, given the small radius of the inclusion, the solution is assumed to be constant on the cross sections and on the border of the cross sections. Thus, given the trace operator $\gamma_{\Gamma} : H^1(D) \cup H^1(\Sigma) \rightarrow H^{\frac{1}{2}}(\Gamma)$, defined as $\gamma_{\Gamma} v = v|_{\Gamma} \forall v \in H^1(D) \cup H^1(\Sigma)$, two extension operators are defined:

$$\mathcal{E}_{\Sigma} : H^1(\Lambda) \rightarrow H^1(\Sigma) \quad \text{and} \quad \mathcal{E}_{\Gamma} : H^1(\Lambda) \rightarrow H^{\frac{1}{2}}(\Gamma),$$

which, given a function $\hat{v} \in H^1(\Lambda)$, uniformly extend the value $\hat{v}(s), s \in [0, S]$ to the cross section $\Sigma(s)$ of the cylinder, i.e. $\mathcal{E}_{\Sigma} \hat{v}(\mathbf{x}) = \hat{v}(s) \forall \mathbf{x} \in \Sigma(s)$, and to the boundary $\Gamma(s)$ of $\Sigma(s)$, i.e. $\mathcal{E}_{\Gamma} \hat{v}(\mathbf{x}) = \hat{v}(s) \forall \mathbf{x} \in \Gamma(s)$. Setting $\hat{V} = H_0^1(\Lambda)$, the following spaces are introduced:

$$\begin{aligned} \tilde{V} &= \{v \in H_0^1(\Sigma) : v = \mathcal{E}_{\Sigma} \hat{v}, \hat{v} \in \hat{V}\}, \quad \mathcal{H}^{\Gamma} = \{v \in H^{\frac{1}{2}}(\Gamma) : v = \mathcal{E}_{\Gamma} \hat{v}, \hat{v} \in \hat{V}\}, \\ V_D &= \{v \in H_0^1(D) : \gamma_{\Gamma} v \in \mathcal{H}^{\Gamma}\} \end{aligned}$$

whose functions satisfy the hypothesis on the regularity of the solution. Denoting by $(\cdot, \cdot)_\star$ the L^2 -scalar product on a generic domain \star and by X' the dual of a generic space X , the weak formulation of (1)-(8) reads: *find* $(u, \tilde{u}) \in V_D \times \tilde{V}$, $\psi \in \mathcal{H}^\Gamma$, $\phi \in \mathcal{H}^{\Gamma'}$ such that

$$(K\nabla u, \nabla v)_D - \langle \phi, \gamma_\Gamma v \rangle_{\mathcal{H}^{\Gamma'}, \mathcal{H}^\Gamma} = (f, v)_D \quad \forall v \in V_D, \quad (9)$$

$$(\tilde{K}\nabla \tilde{u}, \nabla \tilde{v})_\Sigma + \langle \phi, \gamma_\Gamma \tilde{v} \rangle_{\mathcal{H}^{\Gamma'}, \mathcal{H}^\Gamma} = (g, \tilde{v})_\Sigma \quad \forall \tilde{v} \in \tilde{V}, \quad (10)$$

$$\langle \gamma_\Gamma u - \psi, \eta \rangle_{\mathcal{H}^\Gamma, \mathcal{H}^{\Gamma'}} = 0 \quad \forall \eta \in \mathcal{H}^{\Gamma'}, \quad (11)$$

$$\langle \gamma_\Gamma \tilde{u} - \psi, \eta \rangle_{\mathcal{H}^\Gamma, \mathcal{H}^{\Gamma'}} = 0 \quad \forall \eta \in \mathcal{H}^{\Gamma'}. \quad (12)$$

A well posed 3D-1D formulation follows by operating a geometrical reduction of the operators:

$$\langle \phi, \gamma_\Gamma v \rangle_{\mathcal{H}^{\Gamma'}, \mathcal{H}^\Gamma} = \int_\Gamma \phi \gamma_\Gamma v \, d\Gamma = \int_0^S \left(\int_{\Gamma(s)} \phi \gamma_\Gamma v \, dl \right) ds = \int_0^S |\Gamma(s)| \bar{\phi}(s) \check{v}(s) \, ds = \langle |\Gamma| \bar{\phi}, \check{v} \rangle_{\hat{V}', \hat{V}} \quad \forall v \in V_D$$

$$(\tilde{K}\nabla \tilde{u}, \nabla \tilde{v})_\Sigma = \int_\Sigma \tilde{K} \nabla \tilde{u} \nabla \tilde{v} \, d\sigma = \int_0^S \tilde{K} |\Sigma(s)| \frac{d\hat{u}}{ds} \frac{d\hat{v}}{ds} \, ds$$

being $\check{v} \in \hat{V}$ such that $\gamma_\Gamma v = \mathcal{E}_\Gamma \check{v}$, and $\hat{u}, \hat{v} \in \hat{V}$ such that $\tilde{u} = \mathcal{E}_\Sigma \hat{u}$, $\tilde{v} = \mathcal{E}_\Sigma \hat{v}$. The quantities $|\Gamma(s)|$ and $|\Sigma(s)|$ are the measure of $\Gamma(s)$ and $\Sigma(s)$, respectively.

The final PDE-constrained optimization formulation of the problem is derived introducing a cost functional to measure the error in the fulfillment of the coupling conditions (11)-(12), and looking for the solution as the minimum of such functional constrained by the constitutive equations on the various domains:

$$\min_{\bar{\phi}, \hat{\psi}} J = \frac{1}{2} \left(\|\gamma_\Gamma u(\bar{\phi}, \hat{\psi}) - \mathcal{E}_\Gamma \hat{\psi}\|_{\mathcal{H}^\Gamma}^2 + \|\gamma_\Gamma \mathcal{E}_\Sigma \hat{u}(\bar{\phi}, \hat{\psi}) - \mathcal{E}_\Gamma \hat{\psi}\|_{\mathcal{H}^\Gamma}^2 \right) \quad (13)$$

such that, for $\check{v}, \hat{\psi} \in \hat{V}$: $\gamma_\Gamma v = \mathcal{E}_\Gamma \check{v}$ and $\psi = \mathcal{E}_\Gamma \hat{\psi}$:

$$(K\nabla u, \nabla v)_D + \alpha(|\Gamma| \check{u}, \check{v})_\Lambda - \langle |\Gamma| \bar{\phi}, \check{v} \rangle_{\hat{V}', \hat{V}} = (f, v)_D + \alpha(|\Gamma| \hat{\psi}, \check{v})_\Lambda \quad \forall v \in V_D, \quad (14)$$

$$\left(\tilde{K} |\Sigma| \frac{d\hat{u}}{ds}, \frac{d\hat{v}}{ds} \right)_\Lambda + \hat{\alpha}(|\Gamma| \hat{u}, \hat{v})_\Lambda + \langle |\Gamma| \bar{\phi}, \hat{v} \rangle_{\hat{V}', \hat{V}} = (|\Sigma| \bar{g}, \hat{v})_\Lambda + \hat{\alpha}(|\Gamma| \hat{\psi}, \hat{v})_\Lambda \quad \forall \hat{v} \in \hat{V}. \quad (15)$$

In the above equations $\bar{g}(s) = \frac{1}{|\Sigma(s)|} \int_{\Sigma(s)} g \, d\sigma$, and a consistent correction has been introduced, such that, for any $\alpha, \hat{\alpha} > 0$ the problems on the 3D domain and on the 1D domain are well posed independently from the prescribed boundary conditions.

The formulation here shortly described can be generalized to different boundary conditions, to multiple intersecting segments [3] and to different interface conditions [2].

2 Discrete problem

The main novelty content of the present work consists in the use of the XFEM for the discretization of problem (13)-(15). Let us thus extend the domain D to the the whole Ω and let us consider a mesh \mathcal{T} on Ω made of N_τ tetrahedral elements τ_j , i.e. $\mathcal{T} = \bigcup_{j=1}^{N_\tau} \tau_j$, whose position in space is independent from the position of the 1D domain Λ . On this mesh we define linear Lagrangian finite element basis functions $\{\varphi_k\}_{k=1}^N$, and we denote by $\mathcal{I} = \{1, \dots, N\}$ the set of their

indexes. In addition to these *standard* functions, we enrich the discrete approximation space with additional functions. In order to define them, let us introduce a cylinder Δ with centreline coinciding with Λ and having constant cross-section radius $\rho \geq R$. We recall that R is the radius of the inclusion Σ of the original equidimensional problem. Let us further denote by \mathcal{T}_Δ the set of mesh elements having non empty intersection with the cylinder, $\mathcal{T}_\Delta := \{\tau \in \mathcal{T} : \tau \cap \Delta \neq \emptyset\}$, and by $\mathcal{J} := \{k \in \mathcal{I} : \exists \tau_j \in \mathcal{T}_\Delta, \text{supp}(\varphi_k) \cap \tau_j \neq \emptyset\}$, the subset of degrees of freedom indexes k such that the support of the basis function φ_k has a non empty overlap with an element in \mathcal{T}_Δ . Being, finally $d_\Lambda(\mathbf{x})$ the distance of \mathbf{x} from Λ , the following enrichment functions are defined: for $k \in \mathcal{J}$

$$\chi_k(\mathbf{x}) = \varphi_k(\mathbf{x})\zeta(d_\Lambda(\mathbf{x}))r_{\mathcal{J}}(\mathbf{x})$$

where $\zeta(d_\Lambda(\mathbf{x}))$ is chosen according to the results in [7] as:

$$\zeta(d_\Lambda(\mathbf{x})) = \begin{cases} -\log(d_\Lambda(\mathbf{x})) & \text{if } d_\Lambda(\mathbf{x}) > R \\ -\log(R) & \text{if } d_\Lambda(\mathbf{x}) \leq R \end{cases},$$

and $r_{\mathcal{J}}(\mathbf{x}) := \sum_{k \in \mathcal{J}} \varphi_k(\mathbf{x})$ is a so-called ramp function, [5]. Function $\zeta(d_\Lambda(\mathbf{x}))$ is shown in Figure 1 on a plane orthogonal to Λ . At each section the function has a *log-like* behaviour moving radially on planes normal to Λ , at a distance greater than R from the 1D domain, and is instead constant inside the circle of radius R around Λ . The function is constant in the direction parallel to Λ . This introduces the desired irregular behavior in the discrete approximation, being $\zeta(d_\Lambda(\mathbf{x})) \in V_D$.

The discrete approximation of the unknown u is

$$U = \sum_{k \in \mathcal{I}} U_k \varphi_k(\mathbf{x}) + \sum_{k \in \mathcal{J}} W_k (\chi_k(\mathbf{x}) - \chi_k(\mathbf{x}_k)),$$

being \mathbf{x}_k the mesh node such that $\varphi_k(\mathbf{x}_k) = 1$, $k \in \mathcal{J}$. Following the XFEM paradigm [6], the effect of the enrichment functions is local, close to the 1D domain Λ , accordingly to the chosen value of the radius ρ that defines the region Δ . The shifting $-\chi_k(\mathbf{x}_k)$ yields the property $U(\mathbf{x}_k) = U_k$, in all nodes \mathbf{x}_k , $k \in \mathcal{I}$.

Concerning the remaining unknowns, independent meshes, denoted by $\hat{\mathcal{T}}$, \mathcal{T}^ϕ and \mathcal{T}^ψ can be chosen on Λ for variables \hat{U} , Φ and Ψ , representing the discrete counterpart of \hat{u} , $\bar{\phi}$ and $\hat{\psi}$, respectively. The discrete problem is obtained inserting the discrete functions in (13)-(15) and replacing the norms in \mathcal{H}^Γ with norms in $L^2(\Lambda)$ in the functional. The derivation is formally identical to the one provided in [1] and is therefore not reported here.

3 Numerical integration

A key aspect for the successful application of the XFEM lies in the numerical quadrature of the enrichment basis functions. Indeed, given the irregular behavior of such functions, customized strategies need to be adapted, often relying on sub-triangulations conforming to the interfaces. Here a different approach is devised and applied, which exploits the known behavior of function $\zeta(d_\Lambda(\mathbf{x}))$ and which is capable of correctly capture the curvilinear boundary of the interface. With reference Figure 2, let us consider a tetrahedron $\tau \in \mathcal{T}$, partially crossed by the 3D inclusion Σ with centreline Λ , and let us denote by $s_{v_0} \geq s_{v_1} \geq s_{v_2} \geq s_{v_3}$ the curvilinear

abscissas of the projections on Λ of the four vertexes of τ . Then:

$$\int_{\tau} \zeta(d_{\Lambda}(\mathbf{x}))d\mathbf{x} = \int_{s_{v_0}}^{s_{v_3}} \left(\int_{p(s)} \zeta(d_{\Lambda}(\mathbf{x}))d\sigma \right) := \int_{s_{v_0}}^{s_{v_3}} f_{\zeta}(s)ds$$

where $p(s)$ are the polygonal regions given by the intersection of τ with a plane orthogonal to Λ at each $s \in [s_{v_0}, s_{v_3}]$. In each interval $\Lambda^t := [s_{v_t}, s_{v_{t+1}}]$, $t = 0, \dots, 2$, the function representing the surface area of $p(s)$ is smooth and consequently $f_{\zeta}(s)$ is smooth, since $\zeta(d_{\Lambda}(\mathbf{x}))$ is constant on each section on planes parallel to Λ . A Gaussian 1D quadrature rule with n_{Λ} nodes can be thus efficiently adopted to integrate $f_{\zeta}(s)$ in each Λ^t , requiring, the computation of values $f_{\zeta}(s_j)$ at integration nodes $s_j \in (s_{v_t}, s_{v_{t+1}})$, $j = 1, \dots, n_{\Lambda}$. The computation of integrals $f_{\zeta}(s_j) = \int_{p(s_j)} \zeta(d_{\Lambda}(\mathbf{x}))$ on the regions $p(s_j)$ that have an empty intersection with Σ can be performed by standard approaches, whereas, when $p(s_j) \cap \Sigma \neq \emptyset$, integration is performed combining the approaches proposed in [4] and [14], adapted to the present case. Let us denote by \mathbf{x}_{Λ}^j the point at the intersection between Λ and the plane containing $p(s_j)$, and let us further call $p^{\text{in}}(s_j)$ the portion of $p(s_j)$ inside Σ , and by $p^{\text{ext}}(s_j)$ the portion outside Σ . The regions $p^{\text{in}}(s_j)$ and $p^{\text{ext}}(s_j)$ are covered by triangular regions with one vertex in \mathbf{x}_{Λ}^j , as shown in Figure 2, for the particular case of $\Sigma \subset p(s_j)$. However, such covering can be determined also when Σ is only partially contained in $p(s_j)$, more details being available in [4]. On each triangular region, three changes of variables are then performed, which allow to account for the curvilinear portion of the border of the integration domains, and also to cluster the integration nodes where the function has a steep gradient. First, an affine mapping $t : [x, y] \mapsto [x^*, y^*]$ is used to map each region to the reference triangle, in such a way that point \mathbf{x}_{Λ}^j is mapped to the origin of x^*y^* reference system. Consequently, the portion of $\Gamma(s_j)$ contained in the triangle is mapped to an ellipse, centered in the origin of x^*y^* . Then a rotation $\varrho : [x^*, y^*] \mapsto [\tilde{x}, \tilde{y}]$ is used to align the x^*y^* reference system to the principal axis of such ellipse, whose equation can be written as $\frac{\tilde{x}^2}{\lambda_1^2} + \frac{\tilde{y}^2}{\lambda_2^2} = R^2$ in the new axis. Finally we introduce a polar transformation $\Upsilon : [\mathbf{r}, \theta] \mapsto [\tilde{x}, \tilde{y}]$, depending on a parameter q and defined as:

$$\begin{cases} \tilde{x} = \lambda_1 R r^q \cos \theta \\ \tilde{y} = \lambda_2 R r^q \sin \theta. \end{cases}$$

Then n_{θ} Gaussian quadrature points along θ and n_r Gaussian quadrature points along each radial direction are mapped back from this reference frame. According to the chosen value of q , a clustering of the nodes towards the border of the ellipse, where the function has a steep gradient, is obtained, with higher values corresponding to a higher clustering. A value $q = 1$ is used for the regions inside Σ , where $\zeta(d_{\Lambda}(\mathbf{x}))$ is constant whereas a value $q = 3$ is used for the regions outside Σ .

As an example, we integrate function $\zeta(d_{\Lambda}(\mathbf{x}))$ over a unit edge cubic domain, with Λ coinciding with one of the vertical edges of the cube. This simple geometry is chosen to allow for the computation of the exact integral, and two values of R are proposed, $R = 0.1$ and $R = 0.3$. The obtained results are reported Table 1, showing how, with the proposed strategy it is possible to compute the integral up to machine precision. In the table, N_{pt} represents the total number of quadrature points. In this particular case, one single node along Λ is sufficient, given the geometry of the domain and the regularity of the integrated function.

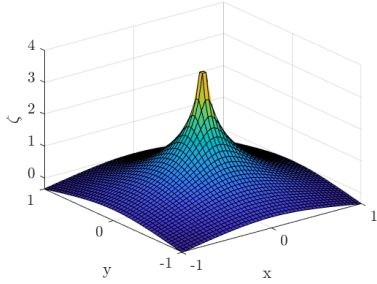


Figure 1: Enrichment function on a section orthogonal to the inclusion centreline

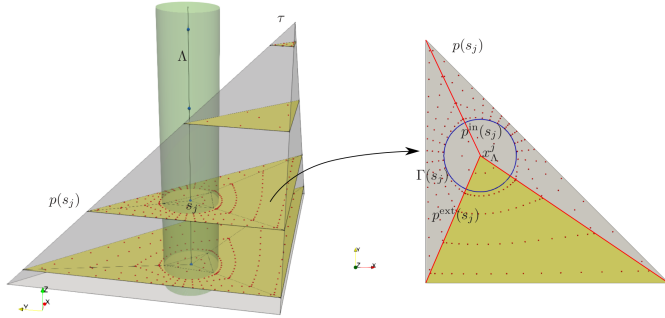


Figure 2: Description of numerical integration strategy

Table 1: Numerical quadrature errors for different numbers of integration points

n_Λ	n_τ	n_θ	N_{pt}	error - $R = 0.1$	error - $R = 0.3$
1	4	9	59	9.85e-08	2.97e-09
1	6	9	111	6.45e-12	1.75e-12
1	8	12	195	4.57e-16	1.67e-16

4 Numerical results and discussion

The numerical examples here reported are obtained using the XFEM approximation space described in Section 2 for the 3D unknown. Equally spaced meshes are instead chosen for the 1D variables and piecewise linear continuous basis functions are used on $\hat{\mathcal{T}}$ for \hat{U} and on \mathcal{T}^ψ for Ψ , whereas piecewise constant basis functions on \mathcal{T}^ϕ are used for Φ . Different choices are however possible. Quadrature formulas with maximum values of $n_\Lambda = 3$, $n_\tau = 5$ and $n_\theta = 16$ are used.

4.1 3D problem with singular source term

In this first example we consider a 3D problem with given source term along a segment. The domain Ω is a cube of edge $l = 2$ centered in the axes origin with boundary $\partial\Omega$, that is split in a region $\partial\Omega_\perp$, given by the union of the faces perpendicular to the z -axis, and a region $\partial\Omega_\parallel = \partial\Omega \setminus \partial\Omega_\perp$. Let Λ be a segment lying on the z -axis and crossing the cube from side to side, intersecting $\partial\Omega_\perp$. We consider problem (9)-(12) in Ω , with $K = 1$, $f = 0$ and a given function $\phi = -\frac{1}{10\pi R}$ on Γ , such that the exact solution is $u_{\text{ex}} = \frac{1}{10\pi} \log(x^2 + y^2)$ in D and $u_{\text{ex}} = \frac{1}{10\pi} \log(R)$ in Σ , and $R = 10^{-3}$. Appropriate Dirichlet boundary conditions are prescribed on $\partial\Omega_\parallel$ and homogeneous Neumann conditions are instead chosen on $\partial\Omega_\perp$. Clearly $u_{\text{ex}} \in V_D$, and we approximate such solution solving equation (14) with $\alpha = 0$ and $\bar{\phi} = \phi$, and using the proposed XFEM approach. Convergence trends against the total number of degrees of freedom N are reported in Figure 3, for the L^2 and H^1 relative errors. Both a classical FEM discretization and the proposed XFEM approach are considered, for four different uniform meshes. In the XFEM cases different enrichment regions are analyzed, determined by increasing the value of the parameter ρ . As expected, sub-optimal convergence rates are obtained with

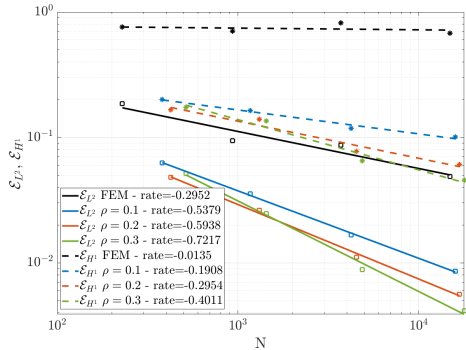


Figure 3: Test 1, trend of the relative errors under mesh refinement. Full lines: relative L^2 -norm of the error; Dashed line: relative H^1 -norm of the error.

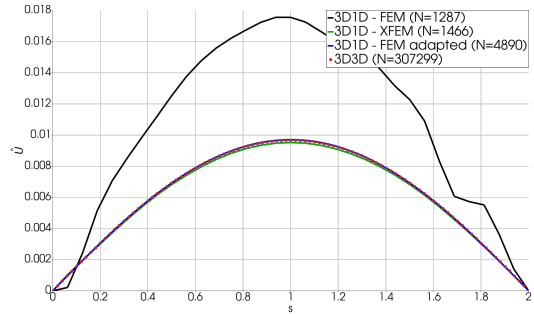


Figure 4: Test 2, Comparison of the solution obtained with standard FEM on the centerline of the inclusion for a 3D3D conforming setting and by means of the 3D-1D reduced model.

standard FEM on uniformly refined meshes. The use of XFEM allows to reduce the error, for any value of $\rho \geq R$, and optimal convergence trends are recovered for $\rho \approx 0.2$. Indeed, it is known in the XFEM literature [6] that, for singular sources, the enrichment of a region independent from the meshsize is necessary for optimal convergence rates. For values of $\rho \geq 0.2$ more than optimal trends are reached thanks to the use of the enrichment in a wider region of the domain.

4.2 3D-1D coupled problem

The second numerical example deals with a coupled 3D-1D problem and is aimed at showing the effectiveness of the proposed approach in avoiding the need for mesh adaptation near the inclusion. At this end, the same numerical test already presented in [1] is re-proposed here: in the original work, it was observed that, for solutions with a high gradient near the inclusion, mesh adaptation is necessary to improve accuracy. The simulation domain Ω is a cube of edge $l = 2$ with an embedded cylindrical inclusion Σ of radius $R = 0.01$ whose centerline Λ lies on the z -axis. The boundary $\partial\Omega$ is split in $\partial\Omega_{\perp}$ and $\partial\Omega_{\parallel}$ as in the previous test. In this domain we solve problem (13)-(15) with $K = 1$, $f = 1$, $\bar{g} = 0$ and a value $\tilde{K} = 10^5$. Homogeneous Dirichlet boundary conditions are prescribed on $\partial\Omega_{\perp}$ and at the segment endpoints, while homogeneous Neumann boundary conditions are set on $\partial\Omega_{\parallel}$. In addition to this, we also consider the fully 3D-3D coupled setting of problem (9)-(12), with the same data. This 3D-3D problem is solved with standard finite elements on a fine mesh conforming to the interface Γ , and is used as reference.

Figure 4 reports four different numerical solutions on the centreline Λ , plotted against line-length: the 3D-3D reference solution to problem (9)-(12) (labeled 3D3D), and the solutions to the 3D-1D problem (13)-(15), obtained with standard finite elements on a uniformly refined mesh (labeled 3D1D - FEM), with the FEM on an adapted mesh refined around the inclusion Λ (labeled 3D1D-FEM adapted) and with the XFEM (labeled 3D1D-XFEM). The total number of degrees of freedom for the 3D meshes is labeled N and is shown in the figure for each case. For the XFEM-based approach a value of $\rho = 0.01$ is used to keep the number of additional

DOFs as low as possible. Concerning the 1D variables, for the 3D1D-FEM and 3D1D-XFEM approaches the number of DOFs for \hat{U} is 31, whereas 17 DOFs are used for Ψ and 16 for Φ ; for the 3D1D-FEM adapted solution, 400 DOFs are used for \hat{U} , 201 for Ψ and 200 for Φ . We can see that, despite using nearly the same number of DOFs of the 3D1D-FEM case, the solution with the XFEM is almost perfectly overlapped to the reference and to the solution on the adapted mesh, which instead require a much higher number of unknowns.

4.3 Conclusions

The proposed enrichment function and integration strategy yields an XFEM formulation for 3D-1D coupled elliptic problems capable of recovering optimal convergence trends of the error and good approximation capabilities on uniformly refined meshes.

Acknowledgements

This work is supported by the MIUR project “Dipartimenti di Eccellenza 2018-2022” (CUP E11G18000350001) and by INdAM-GNCS. Computational resources are partially supported by SmartData@polito.

References

- [1] S. Berrone, D. Grappein, and S. Scialò. “3D-1D coupling on non conforming meshes via a three-field optimization based domain decomposition”. In: *Journal of Computational Physics* 448 (2022), p. 110738. DOI: 10.1016/j.jcp.2021.110738.
- [2] S. Berrone, D. Grappein, and S. Scialò. “A PDE-constrained optimization method 3D-1D coupled problems with discontinuous solutions”. preprint. 2022. eprint: <https://arxiv.org/abs/2203.01732v1>.
- [3] S. Berrone et al. “A gradient based resolution strategy for a PDE-constrained optimization approach for 3D-1D coupled problems”. In: *Int J Geomath* 13.1 (2022). DOI: 10.1007/s13137-021-00192-0.
- [4] S. Falletta and L. Scuderi. “A new boundary element integration strategy for retarded potential boundary integral equations”. In: *Applied Numerical Mathematics* 94 (2015), pp. 106–126. ISSN: 0168-9274. DOI: 10.1016/j.apnum.2015.03.009.
- [5] T. P. Fries. “A corrected XFEM approximation without problems in blending elements”. In: *Internat. J. Numer. Methods Engrg* 75 (2008), pp. 503–532.
- [6] Thomas-Peter Fries and Ted Belytschko. “The extended/generalized finite element method: an overview of the method and its applications”. In: *Internat. J. Numer. Methods Engrg*. 84.3 (2010), pp. 253–304. ISSN: 0029-5981. DOI: <http://dx.doi.org/10.1002/nme.2914>.
- [7] Gjerde, Ingeborg G. et al. “Splitting method for elliptic equations with line sources”. In: *ESAIM: M2AN* 53.5 (2019), pp. 1715–1739. DOI: 10.1051/m2an/2019027.

- [8] Robert Gracie and James R. Craig. “Modelling well leakage in multilayer aquifer systems using the extended finite element method”. In: *Finite Elements in Analysis and Design* 46.6 (2010). The Twenty-First Annual Robert J. Melosh Competition, pp. 504–513. ISSN: 0168-874X. DOI: doi.org/10.1016/j.finel.2010.01.006.
- [9] Luca Heltai and Alfonso Caiazzo. “Multiscale modeling of vascularized tissues via non-matching immersed methods”. In: *International Journal for Numerical Methods in Biomedical Engineering* 35.12 (2019), e3264. DOI: [10.1002/cnm.3264](https://doi.org/10.1002/cnm.3264).
- [10] Tobias Köppl, Ettore Vidotto, and Barbara Wohlmuth. “A 3D-1D coupled blood flow and oxygen transport model to generate microvascular networks”. In: *International Journal for Numerical Methods in Biomedical Engineering* 36.10 (2020), e3386. DOI: [10.1002/cnm.3386](https://doi.org/10.1002/cnm.3386).
- [11] Tobias Köppl et al. “Mathematical modeling, analysis and numerical approximation of second-order elliptic problems with inclusions”. In: *Mathematical Models and Methods in Applied Sciences* 28.05 (2018), pp. 953–978. DOI: [10.1142/S0218202518500252](https://doi.org/10.1142/S0218202518500252).
- [12] Miroslav Kuchta et al. “Analysis and Approximation of Mixed-Dimensional PDEs on 3D-1D Domains Coupled with Lagrange Multipliers”. In: *SIAM Journal on Numerical Analysis* 59.1 (2021), pp. 558–582. DOI: [10.1137/20M1329664](https://doi.org/10.1137/20M1329664).
- [13] F. Laurino and P. Zunino. “Derivation and analysis of coupled PDEs on manifolds with high dimensionality gap arising from topological model reduction.” In: *ESAIM: M2AN* 53.6 (2019), pp. 2047–2080.
- [14] G. Monegato and L. Scuderi. “Numerical integration of functions with boundary singularities”. In: *Journal of Computational and Applied Mathematics* 112.1 (1999), pp. 201–214. ISSN: 0377-0427. DOI: [10.1016/S0377-0427\(99\)00230-7](https://doi.org/10.1016/S0377-0427(99)00230-7).